Research Article

Kinetic Study and Optimization of Tetramethylthionine Chloride Photodegradation by Iron-Perylene MOF with Hydrogen Peroxide Using Response Surface Methodology

Muhammad Fathurrahman
Department of Chemistry, Faculty of Mathematics and Natural Sciences, University of Indonesia, Depok, Jawa Barat, Indonesia
Study Program of Chemistry, Faculty of Mathematics and Natural Sciences, Universitas Pakuan, Bogor, Jawa Barat, Indonesia

Agustino Zulys* and Jarnuzi Gunlazuardi
Department of Chemistry, Faculty of Mathematics and Natural Sciences, University of Indonesia, Depok, Jawa Barat, Indonesia

* Corresponding author. E-mail: zulys@ui.ac.id
DOI: 10.14416/j.asep.2025.02.002
Received: 1 October 2024; Revised: 2 December 2024; Accepted: 21 January 2025; Published online: 7 February 2025

Abstract
This study aimed to synthesize and characterize an iron-perylene metal-organic framework (MOF) as a photocatalyst for the degradation of tetramethylthionine chloride in the presence of hydrogen peroxide. Iron-based MOF with perylene-3,4,9,10-tetra carboxylate (PTC) ligands was produced through a solvothermal technique and was characterized for its morphology, optical properties, surface area, thermal stability, and electrochemical behavior. The results showed that Fe-PTC MOF had a tubular crystalline structure with an average crystal size of 51 nm, a bandgap energy of 1.94 eV, and was responsive to visible light. Thermal analysis revealed a significant weight loss of 63.53% between 390 °C and 490 °C due to the decomposition of the organic linker, with an exothermic heat release of 5.97 J/mg. Electrochemical characterization showed an onset oxidation potential of 0.641 V (vs. Standard Hydrogen Electrode (NHE)) and a calculated Lowest Unoccupied Molecular Orbital (LUMO) energy level of –1.299 V, indicating potential applications in photocatalytic and photovoltaic technologies. Photocatalytic activity tests demonstrated that the degradation of tetramethylthionine chloride followed pseudo-first-order kinetics, and optimization using Response Surface Methodology (RSM) identified the optimal conditions for degradation: 1.5 mg of photocatalyst, 0.2 M H_2O_2 concentration, and 133 min of contact time. These results underscore the effectiveness of Fe-PTC MOF in treating dye-contaminated textile wastewater under illumination with visible light.

Keywords: Metal-organic framework, Photodegradation, Response Surface Methodology, Tetramethylthionine chloride

1 Introduction

Rapid economic and industrial growth, environmental pollution, and energy shortages are essential factors that limit sustainable societal development [1]. One of the industries that is growing is the textile industry, which uses various kinds of chemicals such as dyes, salts, and surfactants in every process, including pretreatment, printing/dyeing, and finishing [2]. According to the World Bank, the textile industry reportedly produces around 17–20% of liquid waste [3]. One type of pollutant in liquid waste is organic dyes, including tetramethylthionine chloride (TMTC), known as methylene blue, and sodium 4-[4-(dimethylamino)phenylazo]benzenesulfonate, known as methyl orange (MO). These dye wastes are toxic, very difficult to degrade and disrupt aquatic ecosystems [4]. To overcome this problem, we need

an effective method to remove organic dyes from textile waste.

Several methods, such as coagulation, electrocoagulation, and adsorption, can reduce the dye content in textile industry waste. Using these methods can cause new problems, namely the production of new phases of pollutants that are more concentrated because their nature only moves dyes from the liquid phase to the solid phase rather than breaking down complex compounds from the dyes [5]. Photocatalysis is an alternative method that uses semiconductor materials to degrade dyes using UV or visible light as the energy source. Until now, the development of semiconductor materials as photocatalysts has been being researched.

Various metal oxide and sulfide semiconductors such as TiO_2, ZnO, CdS, and Fe_2O_3 have been widely used as photocatalysts to treat textile waste [6]. Even though titanium dioxide (TiO_2) has high stability and efficiency as well as low toxicity, it has a high gap energy (3.2 eV), so to activate its photocatalytic properties, large amounts of energy, such as ultraviolet (UV) light are needed. UV rays are carcinogenic, and only 5% of sunlight. Apart from that, this type of photocatalyst has low porosity, so metal sulfides with low stability in water will produce toxic pollutants [7].

A new group of materials, hybrids of organic and inorganic components such as Metal-Organic Frameworks (MOFs), has been developed as photocatalysts and remains an exciting topic for research. The number of organic linkers and metal ion precursors currently available can produce materials more than 20,000 MOFs [8]. MOFs are porous frameworks with porosity that can be adjusted, and their stability in water, acid, and base systems makes this material very useful, especially in processing liquid waste from the textile industry [9]. MOFs can be used as photocatalysts to degrade textile waste like tetramethyl thionine chloride [10]–[14], methyl orange [13], and rhodamine B [15]. Another MOF application is to degrade pharmaceutical waste like metformin [16] using a photocatalysis reaction.

In recent years, integrating perylene dyes as organic linkers in MOFs has opened new avenues for developing materials with unique electronic, optical, and structural properties. Perylene-3,4,9,10-tetracarboxylate (PTC) is particularly notable for its strong absorption and emission in the visible region, making it a promising candidate for various photonic applications. MOFs with high stability can be obtained by selecting appropriate metal and organic linkers. PTC is a ligand containing a carboxyl group, which is known to act as a hard base. According to Pearson's Hard and Soft Acid-Base (HSAB) theory, hard bases will interact strongly with hard acids. One example of a hard acid metal is Fe(III) because it has a high oxidation state [6].

These PTC ligands have been used as organic linkers to build MOFs with metal precursors, such as Y, K, Dy, Sm, Cr, La, Co, and Ni. Y-PTC MOF has been synthesized for photocatalytic applications in breaking down tetramethyl thionine chloride and methyl orange [13]. Cr-PTC MOF was once synthesized for the photodegradation of tetramethyl thionine chloride [11], [12]. Previous studies have explored using PTC-based MOFs, such as Y-PTC and Cr-PTC, to photodegradation organic dyes like TMTC and MO. With a bandgap of 2.23 eV, Y-PTC MOF demonstrated an 85% degradation efficiency for TMTC under visible light over 3 h [13]. Similarly, Cr-PTC MOF, with a bandgap of 2.01 eV, achieved 90% degradation for tetramethylthionine chloride [11]. This study presents Fe-PTC MOF with a lower bandgap energy of 1.94 eV, which is expected to enhance visible light absorption and degradation efficiency.

In addition, K-PTC MOF has also been synthesized for humidity sensor layers [17]. Dy-PTC and Sm-PTC MOF have been synthesized and characterized [18]. La-PTC MOF has been synthesized for dye degradation photocatalysis applications [9], [19]. Co(II) has also been a metal precursor to PTC but in its anhydride form (PTCDA), thus forming an MOF material for analysis of its fluorescence properties [20]. Ni-PTC MOF was once synthesized for hydrogen production photocatalysis applications [21]. Until now, there has been no research on the synthesis and characterization of MOFs based on Fe(III) metal and PTC ligands for the photodegradation of tetramethyl thionine chloride.

This study aims to synthesize iron-based MOF using PTC as an organic linker to characterize its structural, thermal, and surface properties applied as a photocatalyst to degrade tetramethylthionine chloride dye by reviewing the kinetics and optimization of its photodegradation parameters using response surface methodology. Response Surface Methodology (RSM) is a collection of statistical and mathematical techniques designed to optimize processes and analyze the relationships between several independent variables and a response. It is widely used to model and improve complex systems, mainly when multiple

factors interact non-linearly. In this study, RSM was applied using a Box-Behnken design to optimize the photocatalytic degradation of tetramethylthionine chloride by Fe-PTC MOF, with the variables being photocatalyst weight, H_2O_2 concentration, and contact time.

This study proposes using Fe-PTC MOF as a photocatalyst to break down these contaminants under visible light, offering a sustainable alternative. This research addresses environmental concerns by effectively degrading tetramethyl thionine chloride and lays the groundwork for scalable, energy-efficient industrial processes in wastewater management.

2 Materials and Methods

2.1 *Materials*

All chemicals involved in the synthesis were of analytical grade and employed without additional purification. The materials used in this study included $FeCl_3 \cdot 6H_2O$, iron (III) chloride hexahydrate 99% (Merck); NaOH, sodium hydroxide (Merck); perylene -3,4,9,10-tetracarboxylic dianhydride (PTCDA) with a purity of 97% (Sigma-Aldrich); $HCON(CH_3)_2$ dimethylformamide (DMF) (Merck); C_2H_5OH (Merck); Nafion 5% (Sigma-Aldrich); platinum wire; Ag/AgCl; hydrogen peroxide (H_2O_2), tetramethylthionine chloride (TMTC) and distilled water (H_2O).

2.2 *Instrumentations*

The characterization techniques used are a) Fourier Transform Infrared Spectroscopy (FTIR) Prestidge 21 Shimadzu to identify functional groups and confirm the coordination of Fe with PTC; b) Powder X-ray Diffraction (P-XRD) 7000 Maxima-X, to determine the crystalline structure and phase purity; c) Diffuse Reflectance Spectroscopy (DRS) Shimadzu UV 2450, to measure the optical bandgap, d) FESEM Thermo-Scientific Quattro S completed with EDS Detector, to analyze the morphology and elemental composition, e) Thermogravimetric-Differential Thermal Analysis (TG-DTA) and Differential Scanning Calorimetry (DSC) Hitachi STA200RV, to study thermal stability and decomposition behavior; f) Surface Area Analyzer (SAA) Quantachrome NOVA 1200e, to assess the surface area, pore volume, and pore size distribution; g) Cyclic Voltammetry Potentiostat CH1760D.

The photocatalytic reaction was performed using a 250 W mercury lamp. The concentration of the tetramethyl thionine chloride solution was also measured using a Shimadzu UV-Vis spectrophotometer.

2.3 *Preparation of Na-PTC*

A total of 0.5 g of PTCDA was dissolved in 50 mL of distilled water, and then 0.379 g of NaOH was added while stirring with a magnetic stirrer at around 300 rpm for one hour. Following filtration of the greenish solution, the resulting filtrate was treated with an excess of ethanol to induce the formation of a yellow Na-PTC precipitate. The yellow precipitate was then filtered, washed with ethanol until neutral pH was achieved, then oven-dried at 50 °C for 3 h [22]. The Na-PTC powder obtained was then characterized using FTIR.

2.4 *Synthesis of Fe-PTC MOF*

The Fe-PTC MOF synthesis method follows the La-PTC and Ni-PTC MOF synthesis methods, as well as Y-PTC and Cr-PTC [9], [12], [13], [21]. $FeCl_3 \cdot 6H_2O$ and Na-PTC of 2 mmol and 1 mmol were mixed in 5 mL DMF solvent and 25 mL H_2O and stirred at 300 rpm for 45 min. Subsequently, the mixture was placed in a Teflon-lined stainless-steel autoclave and heated at 170 °C for 24 h. Once cooled to room temperature, the resulting crystals were rinsed with distilled water and DMF until a neutral pH was achieved, then oven-dried at 70 °C for 24 h.

2.5 *Photocatalytic activity test of Fe-PTC MOF*

The photocatalytic activity test for the degradation of tetramethyl thionine chloride (TMTC) using Fe-PTC MOF was conducted under both light and dark conditions to evaluate the material's effectiveness as a photocatalyst. Additionally, a photolysis control test was carried out to measure the extent of dye degradation caused solely by the effect of light without the involvement of the photocatalyst.

The experiment dispersed 1 mg of Fe-PTC MOF into 50 mL of a 10 ppm TMTC solution. The mixture was stirred at 300 rpm and illuminated for 3 h using a 250 W mercury lamp as the light source. Afterward, a 10 mL sample was taken and centrifuged, and the dye concentration was measured using a UV-Vis spectrophotometer at 663 nm. The same procedure was repeated under dark conditions but without any light exposure.

2.6 *Kinetics study of tetramethylthionine chloride photodegradation reaction*

Kinetic studies of dye degradation were modeled using these equations: Equation (1) for pseudo-first-order kinetics and Equation (2) for pseudo-second-order kinetics [23].

$$\ln\left(\frac{C_t}{C_0}\right) = k_f t \quad (1)$$

$$\frac{1}{C_t} - \frac{1}{C_0} = k_s t \quad (2)$$

Description:
k_f = pseudo-first order constant (min^{-1})
k_s = pseudo-second order constant (L/mg.min)
C_0 = the initial concentration of TMTC (mg/L)
C_t = [TMTC] at time t during degradation (mg/L)

Next, the data obtained is then plotted $\ln\left(\frac{C_t}{C_0}\right)$ against t for the pseudo-first-order reaction and $\frac{1}{C_t} - \frac{1}{C_0}$ against t for the pseudo-second-order reaction. The line equation and R^2 value are determined and compared for both pseudo-first-order and pseudo-second-order reactions, following the Langmuir-Hinshelwood kinetic model. This comparison helps evaluate which model better describes the dye degradation kinetics, providing insight into the reaction mechanism [24].

2.7 *Optimization of tetramethylthionine chloride photodegradation*

The photodegradation optimization of TMTC dye was conducted using the Response Surface Methodology (RSM) approach, involving three independent variables. Independent variables are the conditions whose influence on the response will be studied. The independent variables in this research are photocatalyst weight, irradiation time, and H_2O_2 concentration.

This research used RSM Box Behnken Design (BBD) in the Minitab application version 19. The three variables to be studied will produce 15 rows of the experimental matrix. The researcher determines each variable's minimum and maximum values, while the middle value is calculated automatically in the application. In this study, the photocatalyst weight had the lowest value of 0.5 mg, the highest value was 1.5 mg, and the middle value was 1 mg. Meanwhile, for the contact time variable, the lowest value is 90 min, the highest is 150 min, and the middle is 120 min. The last variable, H_2O_2 concentration, has the lowest value of 0.1, the highest value of 0.3, and the middle value of 0.2. Meanwhile, the response variable is the percent efficiency of dye degradation.

The relationship between the independent variables (H_2O_2 concentration, photocatalyst dosage, and irradiation time) and the response (degradation efficiency of tetramethylthionine chloride) was modeled using a quadratic equation as part of the Response Surface Methodology (RSM). The model is expressed in Equation (3), as follows:

$$Y = \beta_0 + \sum\beta_i X_i + \sum\beta_{ii} X_i^2 + \sum\beta_{ij} X_i X_j \quad (3)$$

where Y represents the response (degradation efficiency), X_i and X_j are the independent variables, β_0 is the intercept, β_i are the linear coefficients, β_{ii} are the quadratic coefficients, and β_{ij} are the interaction coefficients. This model enables the prediction of degradation efficiency under varying experimental conditions and identifies significant interactions between variables. The coefficients were determined using regression analysis, and the model's adequacy was evaluated through ANOVA, achieving a high correlation coefficient (R^2).

3 Results and Discussion

3.1 *Preparation of Na-PTC from PTCDA*

Na-PTC is produced from perylene-3,4,9,10-tetracarboxylic dianhydride (PTCDA), recognized for its insolubility in water [13]. The conversion of PTCDA into its salt form, Na-PTC, significantly improves its solubility in polar solvents. This enhancement occurs because the reaction with a base, such as sodium hydroxide, introduces ionic characteristics to the molecule, facilitating interaction with polar solvents through ion-dipole forces.

The physical transformation during the synthesis is evident, as the initial dark red PTCDA material is converted into yellow Na-PTC. This distinct color change indicates a successful chemical modification, as the compound's chromophore is altered during the reaction. The synthesis process and its outcome were further validated using Fourier Transform Infrared Spectroscopy (FTIR), as shown in Figure 1. The FTIR analysis shows the loss of anhydride peaks and the

emergence of carboxylate peaks, confirming the formation of Na-PTC.

Figure 1 shows some differences in the FTIR spectrum between PTCDA and Na-PTC. The difference that can be observed is that in the FTIR spectrum of PTCDA, there is a wavenumber of 1778 cm^{-1}, which indicates the stretching vibration of carbonyl (C=O), and a wavenumber of 1026 cm^{-1}, which shows the stretching vibration (C-O) of the cyclic anhydride PTCDA, while this absorption was not found on the FTIR spectrum of Na-PTC. The disappearance of the 1778 cm^{-1} peak in the FTIR spectrum of Na-PTC is attributed to the hydrolysis of the anhydride groups in PTCDA. During the reaction with NaOH, the anhydride groups are converted into carboxylate groups ($-COO^-$), resulting in the loss of the characteristic C=O stretching vibration at 1778 cm^{-1}. New peaks confirm this transformation at 1603 cm^{-1} and 1418 cm^{-1}, corresponding to carboxylate groups' asymmetric and symmetric stretching vibrations. These findings validate the successful synthesis of Na-PTC through the hydrolysis process [25].

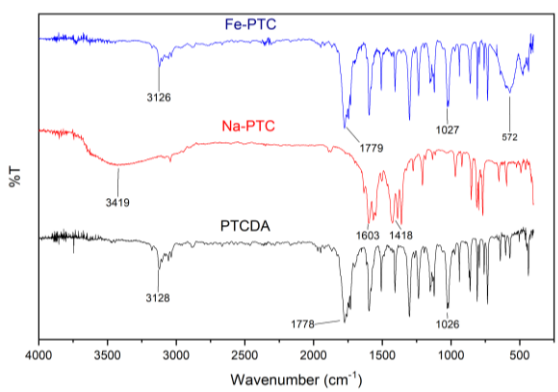

Figure 1: FTIR spectra of Fe-PTC, Na-PTC, and PTCDA.

In the FTIR spectrum of Na-PTC, stretching vibrations of the hydroxyl group (-OH) were also detected at wave numbers around 3419 cm^{-1}. It can be assumed that there are anhydride groups from PTCDA that have been opened, but then some of them do not bind Na^+ cations but instead form carboxylic groups (-COOH) when washing the material with ethanol until the pH is neutral. This hydroxyl absorption overlaps with the stretching vibration of aromatic CH on the perylene group of Na-PTC. Another indication that Na-PTC has formed is the difference in the FTIR spectrum with PTCDA in the fingerprint area, namely the area below 1400 cm^{-1}.

Distinct changes in the FTIR spectrum confirm the transformation from PTCDA to Na-PTC. The characteristic anhydride C=O stretch of PTCDA at 1778 cm^{-1} disappears, while new peaks at 1603 cm^{-1} and 1418 cm^{-1}, corresponding to the asymmetric and symmetric stretching of carboxylate ($-COO^-$) groups, emerge. This transformation is attributed to the nucleophilic attack of hydroxide ions (OH^-) on the anhydride bonds of PTCDA, leading to the opening of the cyclic structure and the formation of Na-PTC through an SN_2 mechanism. The reaction mechanism can be seen in Figure 2. Similar changes have been observed in previous studies on the conversion of PTCDA to its salt forms, further validating these results [13].

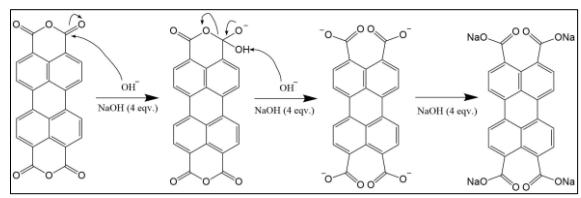

Figure 2: The reaction mechanism of hydrolysis of PTCDA to Na-PTC.

3.2 *Synthesis of MOF Fe-PTC*

The Fe-PTC MOF was prepared through a solvothermal process, utilizing water and DMF solvent mixture for its high boiling point and thermal stability [26]. This solvent mixture system of water and DMF aims to minimize the formation of crystal defects while MOF synthesis is in progress [9], apart from that, DMF also causes the crystal size to become more prominent. Reducing the volume of DMF can cause a decrease in the mass of the crystals formed and less homogeneity, as in research on the synthesis of Cu-BTC MOF [27].

The MOF material formed is red Fe-PTC. This is different from the previous material, Na-PTC, which is yellow. This may indicate that the synthesis of the Fe-PTC MOF was successful. Additional supporting evidence for the successful synthesis of Fe-PTC MOF can be found in the FTIR spectrum data presented in Figure 1. In the FTIR spectrum of the Fe-PTC MOF, an absorption peak at 572 cm^{-1} is noted, indicating the presence of Fe-O vibrations. The same thing was reported in research on the Fe-BDC MOF synthesis, which found absorption at 556 cm^{-1}, indicating symmetric stretching vibration of Fe-O [28].

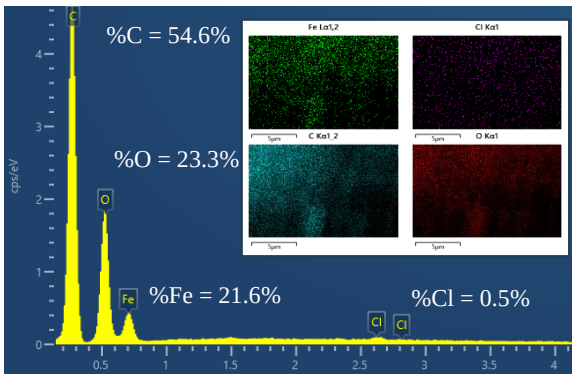

Figure 3: EDS spectrum and mapping of the composition of the elements that make up the Fe-PTC MOF.

The elemental composition and distribution of the Fe-PTC MOF were analyzed using Energy Dispersive Spectroscopy (EDS) and elemental mapping, as shown in Figure 3. The EDS spectrum confirms the presence of critical elements, including Fe (21.6%), C (54.6%), O (23.3%), and a trace amount of Cl (0.5%). The high carbon and oxygen content is attributed to the PTC ligand. In contrast, the iron content indicates the successful incorporation of Fe(III) as the central metal in the MOF structure. The trace presence of chlorine is likely due to residual chloride ions from the synthesis process, such as NaCl by-products during the washing steps.

The elemental mapping further illustrates the uniform Fe, C, and O distribution within the MOF material. The consistent spatial overlap of these elements supports the homogeneity of the Fe-PTC MOF and suggests effective coordination between the PTC ligand and Fe(III). Interestingly, the trace chlorine appears localized, which may indicate incomplete removal during purification. This observation highlights the importance of optimizing washing steps to improve sample purity.

The distribution pattern of Fe is crucial as it directly correlates to the active sites responsible for the photocatalytic activity. The elemental mapping thus validates the synthesis method and provides insights into the material's structural uniformity.

The Cl peak in Figure 3 exhibits a very low intensity, nearly indistinguishable from the baseline. This is likely due to the trace amounts of residual chloride ions (Cl^-) originating from the $FeCl_3 \cdot 6H_2O$ precursor used during synthesis. Despite multiple washing steps, small quantities of Cl^- may remain trapped in the material. The low intensity of the Cl peak also reflects the washing process's efficiency and the Fe-PTC MOF's high purity. Furthermore, the negligible presence of Cl does not significantly affect the structural or functional properties of the material, as confirmed by subsequent characterization and photocatalytic studies.

3.3 *X-ray diffraction of Fe-PTC MOF*

Understanding the crystallinity of the material is crucial, as it is closely linked to its photocatalytic activity [12]. The higher the degree of crystallinity, the smaller the crystal defects. Crystal defects act as recombination centers between electrons and holes, which cause a decrease in photocatalytic activity [29]. So, it can be concluded that the higher the value of a photocatalyst's degree of crystallinity, the more the recombination process is inhibited, resulting in higher photocatalytic activity.

Figure 4 shows that the Fe-PTC MOF material is polycrystalline as indicated by 17 main diffraction peak centers at 9.02º, 12.66º, 24.12º, 24.88º, 25.34º, 27.68º, 31.74º, 33.16º(highest), 35.64º, 40.88º, 45.52º, 49.48º, 54.06º, 57.52º, 62.42º, 64.02º, and 71.96º. The indices of Fe in Fe-PTC cannot be presented, as we consider it a novel material and did not obtain a single crystal. Our assumption of it being a new material is based on the intensities of the diffraction peaks.

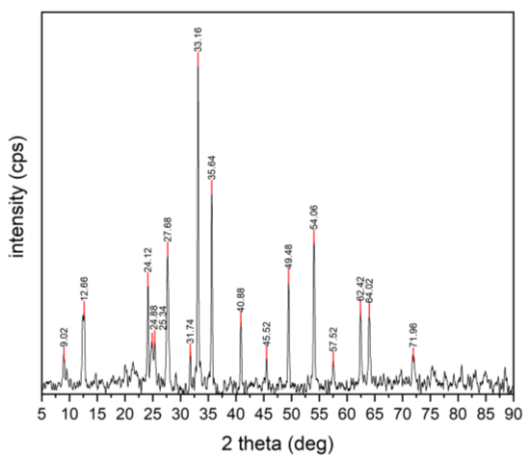

Figure 4: Diffractogram pattern of Fe-PTC MOF.

The Fe-PTC MOF diffractogram shown in Figure 4 is the result of processing from the Origin Version 2018 software, which has undergone a baseline correction and smoothing process using the Savitzky-Golay method and a Point of Window value of 20 pts. Based on the degree of crystallinity

calculation, namely by comparing the area of the main diffraction peak with the area of all peaks, the degree of crystallinity obtained for the Fe-PTC MOF material synthesized in this study is 46.56%. The crystal size was determined using the Debye-Scherrer equation. The calculation results indicate that the average crystal size of the Fe-PTC MOF material is 50.9 nm. This value is twice as significant as the Cr-PTC MOF crystal size, which is 25.7 nm [12].

A mixture of water and DMF influences the formation of Fe-PTC MOF crystals as solvents in solvothermal synthesis. DMF aids in forming Fe-PTC MOF crystals by regulating the deprotonation level of the carboxylate organic linker of PTC. Furthermore, the solvothermal method, which operates at temperatures exceeding the boiling point of the solvent, is used to regulate the crystal growth rate by lowering the activation energy barrier in the reaction between organic linkers and metal ions [30].

The XRD diffractogram of the synthesized MOFs was analyzed to detect potential impurities, which could impact their photocatalytic performance by introducing electron-hole recombination centers, altering structural and electronic properties, or synergistically affecting the photocatalytic activity depending on the interaction conditions [31].

Comparison with standard diffraction patterns revealed no matches with FeO (JCPDS No. 06-0615), which is inherently unstable and tends to oxidize into more stable forms like Fe_2O_3 or Fe_3O_4 [32]. For Fe_2O_3 (JCPDS No. 33-0664), the dominant peak at 33.1° was closely matched by peaks at 33.16° and 33.32° for Fe-PTC and Fe-PTC-HIna, respectively. However, SEM analysis showed rod-shaped morphology inconsistent with Fe_2O_3, typically appearing as hexagonal plates or spheres. Additionally, EDS data for Fe-PTC (Fe: 21.6%, O: 23.3%) and Fe-PTC-HIna (Fe: 6.693%, O: 23.277%) deviated significantly from the theoretical Fe_2O_3 composition (Fe: 69.9%, O: 30.1%), confirming the absence of Fe_2O_3 impurities.

Similarly, for Fe_3O_4 (JCPDS No. 19-0629), the primary peak at 35.4° was near the observed peaks at 35.64° and 35.78°, but no secondary peaks were found. SEM results further indicated no spherical or cubic aggregates typical of Fe_3O_4. EDS data also showed Fe and O compositions incompatible with Fe_3O_4 (Fe: 72.4%, O: 27.6%). These findings suggest that Fe is present as part of the MOF structure rather than as Fe_3O_4 impurities.

Thus, based on XRD, SEM, and EDS analyses, no FeO, Fe_2O_3, or Fe_3O_4 impurities were detected in the synthesized Fe-PTC and Fe-PTC-HIna MOFs.

3.4 *Morphology of Fe-PTC MOF*

Figure 5 shows that the morphology of the Fe-PTC MOF is shaped like a cylindrical tube. This shape is almost the same as Cr-PTC MOF [11], [12] and La-PTC [9], which also have a cylindrical shape. However, the morphological appearance of Fe-PTC MOFs shows numerous impurities, likely due to the omission of a washing step during the synthesis process.

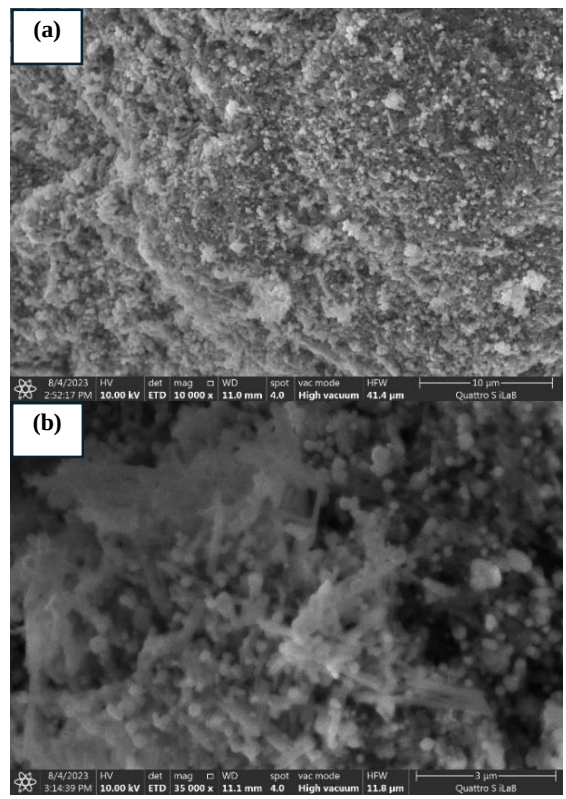

Figure 5: Morphology of Fe-PTC MOF magnification (a) 10,000x, (b) 35,000x.

3.5 *Surface area and pore analysis of Fe-PTC MOF*

The Brunauer-Emmett-Teller (BET) analysis was conducted to evaluate the Fe-PTC sample's specific surface area, pore volume, and pore size distribution, as well as critical parameters for understanding its textural properties and potential applications. These characteristics provide insights into the material's adsorption capacity and catalytic efficiency. The analysis results are depicted in Figure 6, which presents the BET adsorption-desorption isotherm curve of the Fe-PTC MOF.

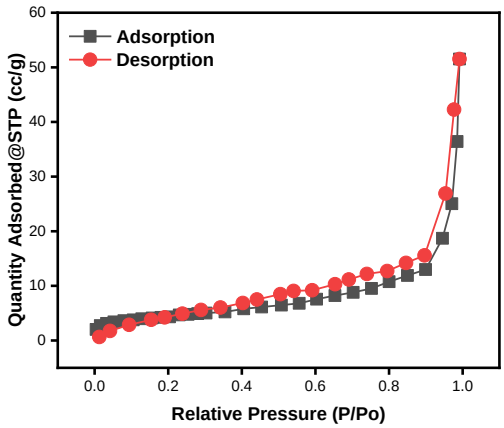

Figure 6: BET Adsorption-Desorption Isotherm Curve of Fe-PTC MOF.

In Figure 6, the desorption curve lies below the adsorption curve, an unusual behavior typically contrary to the hysteresis phenomenon. This discrepancy could be attributed to the specific structural properties of Fe-PTC MOF, such as pore flexibility or the presence of microstructural defects. Alternatively, experimental fluctuations, such as slight variations in temperature or pressure during measurement, may have influenced the desorption process. Further investigations are needed to understand this behavior comprehensively.

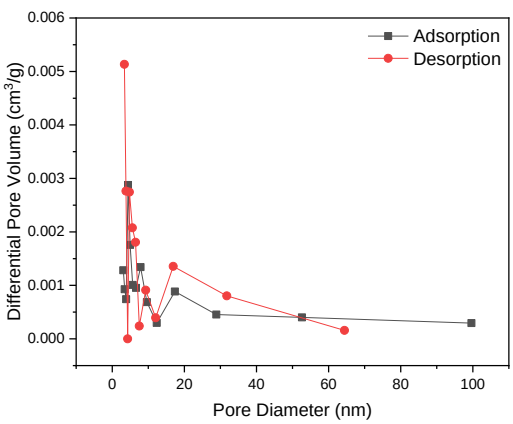

Figure 7: BJH Pore Size Distribution of Fe-PTC MOF.

Figure 7 shows the pore size distribution of Fe-PTC MOF based on BJH analysis for adsorption and desorption. The distribution indicates a mesoporous structure with dominant pore sizes below 50 nm. The desorption curve exhibits minor deviations, which may indicate unique pore dynamics or hysteresis effects during the process. These findings align with the material's application as a photocatalyst, where mesoporous structures enhance accessibility to active sites and facilitate diffusion of reactants and products.

The BET surface area of Fe-PTC MOF was found to be 15.36 m^2/g, which is relatively low compared to other MOFs. This lower surface area can be attributed to several factors. First, the synthesis conditions, including temperature and solvent choice, may influence the development of the porous framework. Second, particle aggregation during the synthesis or drying process could reduce the accessibility of pores. Third, the inherent structural properties of Fe-PTC MOF, with a potential dominance of mesopores over micropores, may also contribute to the lower surface area. Additionally, residual synthesis by-products or incomplete activation could partially block the pores. Further optimization of synthesis parameters could enhance the surface area and improve the material's performance.

The total pore volume, measured for pores, was 0.07971 cc/g. The average pore diameter, calculated using the total pore volume and BET surface area, was 20.76 nm. Table 1 compares the pore analysis and surface area results of Fe-PTC MOF with those of other MOF samples reported in previous studies.

Table 1: Surface Area (S_{BET}), Pore Volume (Vp), and Pore Diameter (Dp) values of PTC-based MOFs.

MOF Material	S_{BET} (m^2/g)	V_p (cm^3/g)	D_p (nm)	Ref.
Ni-PTC	69.779	0.1700	4.25	[21]
Y-PTC	47.749	-	25.00	[13]
La-PTC	22.236	0.0685	12.33	[9]
Fe-PTC	15.358	0.0797	20.76	This Study

Based on Table 1, Fe-PTC MOF has the smallest surface area value; this will, of course, impact its adsorption capacity. Meanwhile, for pore diameter, all MOF samples are in the range of 2–50 nm, where MOF samples are included in mesoporous materials [33]. Mesoporous materials offer advantages as semiconductors because their short distances help reduce or prevent the recombination of excited electrons and holes, enhancing their efficiency [13].

The textural properties of Fe-PTC MOF, including BET surface area (S_{BET}), pore volume (Vp), and average pore diameter (Dp), were compared to those of Y-PTC and La-PTC MOFs, which are commonly used in photocatalytic applications. Fe-PTC MOF exhibited a BET surface area of 15.358 m^2/g, lower than Y-PTC (47.749 m^2/g) and La-PTC

(22.236 m^2/g). This relatively lower surface area could limit the number of active adsorption sites available for photocatalytic reactions.

However, Fe-PTC MOF demonstrated a larger average pore diameter (20.76 nm) compared to Y-PTC (25.00 nm) and La-PTC (12.33 nm), indicating a mesoporous structure that facilitates the diffusion of larger dye molecules. This property is advantageous in photocatalytic applications involving pollutants with bulky structures, as it enhances the accessibility of active sites within the material.

Furthermore, Fe-PTC MOF achieved a higher degradation efficiency (97% for TMTC under visible light irradiation in the presence of H_2O_2 within 120 min) compared to Y-PTC (91.17% for TMTC in 240 min) [13] and La-PTC (67.02% for TMTC in 240 min) [9]. This superior performance can be attributed to its mesoporous structure's synergistic effects and Fe centers' catalytic activity, which facilitate Fenton-like reactions and the generation of hydroxyl radicals (·OH).

Overall, the combination of mesoporosity, moderate pore volume (Vp = 0.0797 cm^3/g), and the active role of Fe centers compensate for the relatively low surface area of Fe-PTC MOF, making it a highly effective photocatalyst.

3.6 *Gap energy of Fe-PTC MOF*

The gap energy is the energy difference between the conduction band and the valence band, representing the maximum energy involved in the electron excitation process [12].

Figure 7 demonstrates that the Fe-PTC MOF exhibits a bandgap energy of 1.94 eV for the direct allowed transition system. If calculated using the max plank Equation (4) to find the maximum wavelength, the value is obtained λ_{max} of 638 nm for direct allowed transition. This shows that the Fe-PTC MOF material produced is responsive to visible light, and the electronic transition that occurs is purely due to interactions between photons and electrons [34].

$$E=\frac{hc}{\lambda} \quad (4)$$

The π-π* orbital transition between the conjugated double bonds in the perylene organic linker influences the low energy gap. This can be compared with Fe-BDC MOF, which has a gap energy value of 2.73 eV [35]. Benzene dicarboxylate (BDC) also has conjugated double bonds, but not as many as perylene tetra carboxylate (PTC), which causes the gap energy value of Fe-PTC to be lower than that of Fe-BDC.

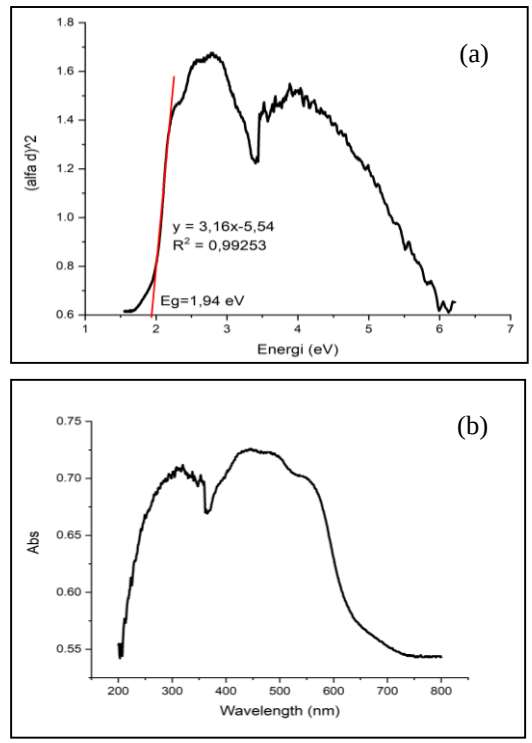

Figure 7: (a) Tauc plot of Fe-PTC MOF and (b) absorbance spectrum.

The bandgap energy of MOFs is also affected by the size of the metal ion cluster. As the cluster size increases and more electrons are added, the number of electrons in the HOMO energy level rises, which results in a smaller energy gap between the valence and conduction bands [36].

The bandgap energy of Fe-PTC MOF was determined to be 1.94 eV, as shown in the Tauc plot (Figure 7(a)). This value falls within the optimal range for photocatalytic materials (1.5–3.0 eV), enabling effective absorption of visible light for photocatalytic applications. The relatively low bandgap energy of Fe-PTC MOF compared to other PTC-based MOFs, such as Cr-PTC (2.01 eV) [11] and La-PTC (2.21 eV) [9], suggests a higher visible light absorption efficiency.

The lower bandgap energy of Fe-PTC MOF can be attributed to the enhanced π-π* orbital transitions in the PTC ligand, as well as the electronic contributions of Fe(III), which has a higher number of d-electrons compared to Cr(III) or La(III). This phenomenon facilitates a smaller energy difference

between the conduction and valence bands, thereby improving its ability to generate photoexcited electron-hole pairs under visible light irradiation.

The bandgap energy of Fe-PTC MOF is also closely related to its photocatalytic performance. Previous studies on Cr-PTC and Y-PTC MOFs demonstrated significant photodegradation of dyes with bandgap values of 2.01 eV and 2.23 eV, respectively. The smaller bandgap of Fe-PTC MOF (1.94 eV) implies a potentially higher photocatalytic activity, as it allows the material to utilize a broader spectrum of visible light, increasing the generation of reactive oxygen species responsible for dye degradation.

Table 2 highlights the bandgap values and maximum absorption wavelengths of PTC-based MOFs. Fe-PTC MOF's maximum absorption wavelength of 638 nm further reinforces its responsiveness to visible light, making it an effective photocatalyst for environmental remediation applications.

Table 2: Gap energy values of PTC-based MOFs.

MOFs	λ_{max} (nm)	Eg (eV)	Ref.
Ni-PTC	514	2.41	[21]
Y-PTC	563	2.23	[13]
La-PTC	561	2.21	[9]
Dy-PTC	568	2.18	[18]
Sm-PTC	564	2.19	[18]
Cr-PTC	616	2.01	[11]
Fe-PTC	638	1.94	This study

A comparison of the bandgap energy values and maximum wavelengths from previous studies using PTCDA ligand bases is presented in Table 1. Previous studies have shown that the bandgap energy of Cr-PTC MOF is measured at 2.01 eV [11], which is higher than the bandgap energy of Fe-PTC MOF, recorded at 1.94 eV. This is because the number of electrons for the Fe(III) metal ion at the HOMO energy level is more significant than for the Cr(III) metal ion.

A photocatalyst's energy bandgap (Eg) significantly impacts its ability to harness light energy for photocatalytic reactions. Fe-PTC MOF exhibited a bandgap energy of 1.94 eV, which lies in the visible light spectrum. This low bandgap energy enhances its photocatalytic performance by enabling the absorption of a broader range of visible light wavelengths, thereby generating more electron-hole pairs for photocatalytic reactions.

In comparison to other MOFs with PTC-based linkers, such as Y-PTC (Eg=2.20 eV) and La-PTC (Eg=2.21 eV), Fe-PTC MOF's lower bandgap energy offers a distinct advantage under visible light conditions. The reduced bandgap facilitates more efficient photoexcitation of electrons from the valence band to the conduction band, increasing the availability of reactive species, such as hydroxyl radicals (·OH) and superoxide anions ($\cdot O_2^-$)

Additionally, Fe-PTC MOF's photocatalytic degradation efficiency for TMTC (97% in 120 min) surpasses that of Y-PTC (91.65% in 240 min) and La-PTC (67.02% in 240 min). This demonstrates the critical role of its narrower bandgap in improving light absorption and catalytic activity. Thus, combining low bandgap energy and the synergistic effects of Fe-based catalytic activity enables Fe-PTC MOF to achieve superior photocatalytic efficiency under visible light.

3.7 *Thermal analysis of Fe-PTC MOF*

The thermogravimetric analysis (TGA) data were used to calculate the percentage mass loss at each experiment stage, using Equation (5).

$$\%\text{Mass loss} = \frac{\text{Initial mass} - \text{Final mass}}{\text{Initial mass}} \text{ x } 100\% \quad (5)$$

Figure 8 shows the TG analysis of Fe-PTC MOF, with an initial weight of 3.400 mg, which was conducted from 30 °C to 550 °C at a heating rate of 10 °C/min under a nitrogen atmosphere. The TGA curve indicates a significant weight loss, highlighting the thermal degradation stages of the sample. The initial weight loss begins at around 100 °C, attributed to the loss of adsorbed moisture and volatile compounds, most likely the evaporated water with a percentage of 0.04%. The primary weight loss occurred between 390 °C and 490 °C, indicating the decomposition of PTC as an organic linker with a percentage of 63.53%. The remaining mass at the end of the analysis signifies the non-volatile residue of the sample, which is thought to be iron metal.

The differential scanning calorimetry (DSC) data was used to quantify the heat flow during the exothermic decomposition. Figure 9 shows the enthalpy change, determined from the area under the exothermic peak in the DSC curve and calculated as -5.97 W.s/mg. We can convert the unit to J/mg because they are equivalent. This exothermic behavior suggests a decomposition reaction occurring within the sample, consistent with thermal degradation.

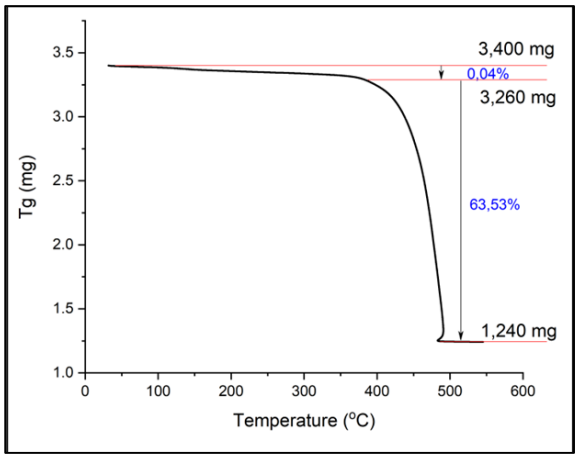

Figure 8: Thermogravimetric curve of Fe-PTC MOF.

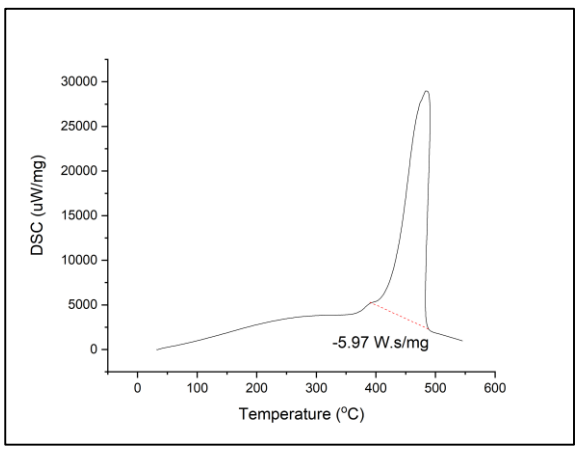

Figure 9: DSC curve of Fe-PTC MOF.

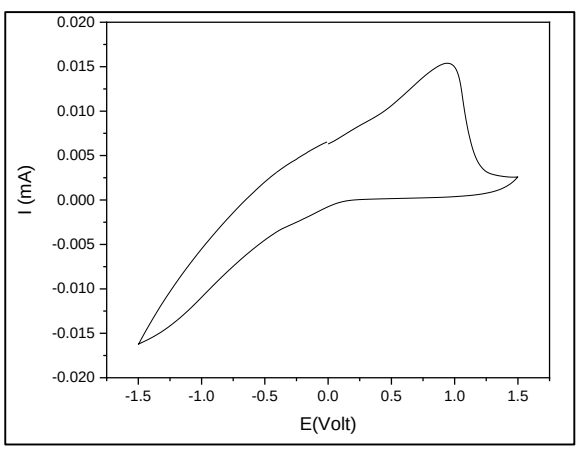

Figure 10: Voltammogram of Fe-PTC MOF.

The thermal degradation pattern of Fe-PTC MOF, as observed in Figures 8 and 9, aligns with similar studies on PTC-based MOFs. For instance, Zulys *et al.* reported a significant weight loss at 376.39 °C for La-PTC MOF, attributed to the decomposition of the PTC ligand and the breakdown of the metal-carboxylate framework [9]. While the decomposition temperature of Fe-PTC MOF (390 °C to 490 °C) is slightly higher, this could be due to differences in the metal-ligand bond strength and the thermal stability conferred by Fe(III). These findings confirm that the thermal stability of Fe-PTC MOF is comparable to other MOFs with PTC ligands, further supporting its potential application in photocatalysis under ambient conditions.

3.8 *Electrochemical characterization of Fe-PTC MOF*

Our study employed cyclic voltammetry (CV) to investigate the electrochemical properties of a Metal-Organic Framework (MOF) based on Fe-PTC. The working electrode was prepared by forming a paste of MOF Fe-PTC with 5% Nafion and applying it onto a fluorine-doped tin oxide (FTO) substrate. A platinum (Pt) wire served as the counter electrode, and an Ag/AgCl electrode was used as the reference. The electrochemical measurements were conducted under the following conditions: initial and final potentials were set at 0 mV, with a step width of 20 ms. The potential was swept from –1500 mV to +1500 mV and back within a current range of 20 mA.

Based on Figure 10, the cyclic voltammetry analysis of Fe-PTC MOF revealed the onset oxidation potential at 0.444 V vs Ag/AgCl, which, when converted to the Standard Hydrogen Electrode (NHE) scale, corresponds to 0.641 V. This potential is indicative of the Highest Occupied Molecular Orbital (HOMO). The DRS UV-Vis analysis determined a band gap of 1.94 eV. Coupled with the oxidation onset potential indicating the HOMO level at 0.641 V versus NHE, the Lowest Unoccupied Molecular Orbital (LUMO) is calculated to be approximately –1.299 V versus NHE. These values indicate the electronic transitions within the MOF structure, highlighting its potential applications in photovoltaic and photocatalytic technologies. In comparison, Ni-MOFs displayed a HOMO level at 0.78 V versus NHE and a LUMO at –1.63 V versus NHE, emphasizing their suitability for hydrogen production under UV-visible light irradiation [21]. Furthermore, La-MOFs demonstrated a LUMO potential of –2.0735 V versus NHE and a band gap of 1.93 eV, enhancing their capability for visible light absorption and proton reduction [37]. These comparative insights underline

the influence of different central metals and organic linkers on the electrochemical properties of MOFs and how these variations can tailor the material's functionality for specific energy-related applications.

3.9 *Photocatalytic activity of Fe-PTC MOF*

The percentage of photocatalytic activity was determined using Equation (6), which accounts for the percentage of degradation (%D), the initial concentration of the sample (C_0) before irradiation, and the final concentration (C_t) after irradiation. The efficiency formula was applied using the concentration values of tetramethylthionine chloride.

$$\%D = \frac{C_0 - C_t}{C_0} x\ 100\% \quad (6)$$

Figure 11 shows that the Fe-PTC MOF does not have significant photocatalytic activity when seen from the comparison of curves in light and dark conditions and photolysis. This indicates that direct photocatalytic degradation by Fe-PTC MOF of tetramethylthionine chloride (TMTC) is very energetically unfavorable. A similar thing also happens when La-PTC MOF is used to degrade rhodamine B and tetramethylthionine chloride dyes. The inappropriate position of the conduction band and valence band causes the electron-hole pairs to experience recombination so that the radical species responsible for degrading the dye are not formed [9].

The percentage of degradation (%D) of TMTC was seen when TMTC was added to peroxide alone. The %D increased again if peroxide was added with Fe-PTC MOF. The highest degradation efficiency (97%) was observed after 120 min of visible light irradiation in the presence of 0.2 M H_2O_2 and 1 mg of Fe-PTC MOF. In contrast, degradation under dark conditions was negligible, indicating the crucial role of light in activating the photocatalyst. Adding H_2O_2 significantly enhanced the degradation efficiency compared to photolysis alone, as it promotes the generation of reactive oxygen species.

Hydrogen peroxide (H_2O_2) is critical in enhancing the photocatalytic degradation process with Fe-PTC MOF. Upon light irradiation, H_2O_2 decomposes into highly reactive hydroxyl radicals (·OH), breaking dye molecules into non-toxic compounds. Additionally, H_2O_2 acts as an electron scavenger, reducing electron-hole recombination and increasing reactive oxygen species' availability. Furthermore, the Fe centers in Fe-PTC MOF may facilitate the activation of H_2O_2 through Fenton-like reactions, further amplifying the generation of hydroxyl radicals. These combined effects significantly enhance the degradation efficiency, as observed in the present study [13].

Compared to La-PTC MOF, which achieved 85% degradation under similar conditions [9], Fe-PTC MOF outperforms due to its lower bandgap energy of 1.94 eV, which enables more efficient visible light absorption and electron-hole pair generation.

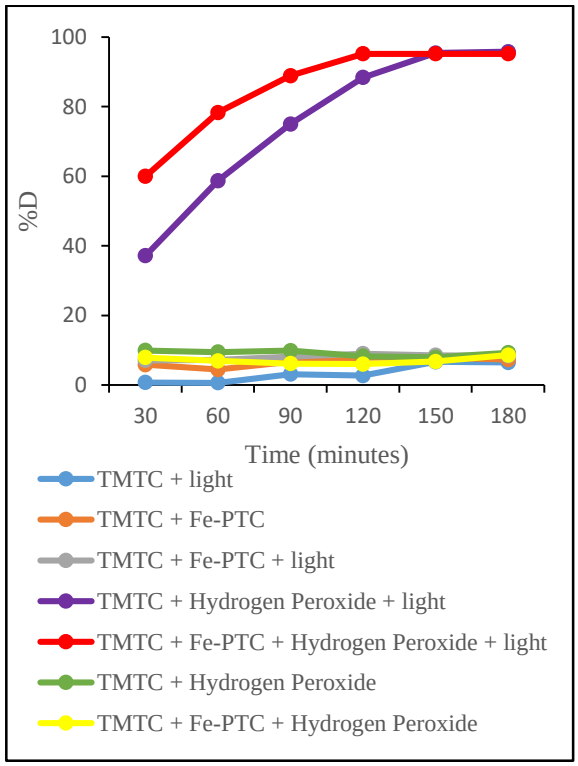

Figure 11: Photolysis and Photocatalysis Activity of Fe-PTC MOF under light and dark conditions and the addition of Hydrogen Peroxide.

3.10 *Kinetics study of tetramethylthionine chloride photodegradation*

The Langmuir-Hinshelwood equation is frequently applied to explain the reaction rate in heterogeneous photocatalysis. Up to now, the breakdown of organic pollutants has generally been examined using pseudo-first-order and pseudo-second-order kinetic models [24]. The rate constants indicated a strong alignment between the model and the experimental data, with correlation coefficients (R^2) as high as 0.9 [38].

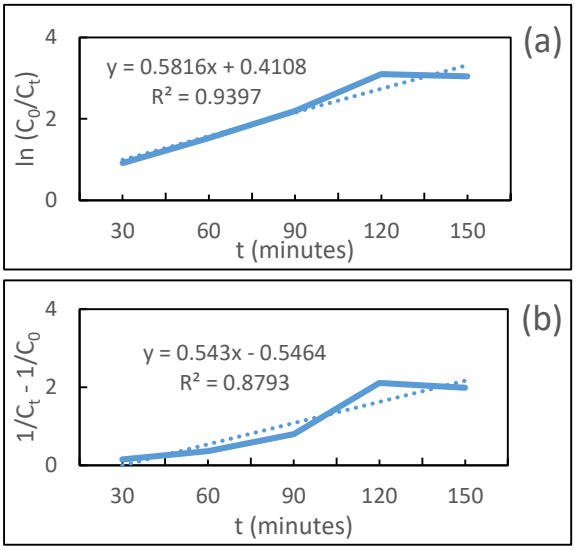

Figure 12: Linear expression of pseudo-first (a) and pseudo-second (b) order rate constant.

Based on Figure 12, the photodegradation reaction follows pseudo-first-order kinetics. The reaction rate constant is 0.5816 min^{-1}, and the R^2 value of 0.9397 indicates a strong fit of the linear model to the experimental data, confirming that the photodegradation process adheres well to first-order kinetics over the observed time.

The photodegradation of tetramethylthionine chloride using Fe-PTC MOF in the presence of H_2O_2 follows pseudo-first-order kinetics, indicating that the concentration of H_2O_2 is in significant excess compared to tetramethylthionine chloride. This excess allows the concentration of H_2O_2 to be treated as effectively constant throughout the reaction, making the photodegradation rate dependent mainly on the concentration of tetramethylthionine chloride. As a result, the overall rate law can be simplified to resemble first-order behavior concerning tetramethylthionine chloride. The observed rate constant (k′) obtained from the kinetic analysis reflects a combination of the actual rate constant (k) and the concentration of H_2O_2, where $k'=k[H_2O_2]$. This pseudo-first-order behavior greatly simplifies the experimental analysis, as a linear plot of $\ln(C_0/C_t)$ versus time provides a straightforward method to determine the rate constant. The catalytic role of Fe-PTC MOF is evident in this process, as it facilitates the decomposition of H_2O_2 to generate reactive oxygen species, such as hydroxyl radicals (·OH), which drive the photodegradation reaction. This finding confirms the effective catalytic activity of Fe-PTC MOF in the photodegradation system.

3.11 *Optimization of tetramethylthionine chloride photodegradation using Fe-PTC MOF in the presence of hydrogen peroxide (H_2O_2)*

The results obtained on the photocatalytic activity of the Fe-PTC MOF in the presence of H_2O_2 were then optimized using the Response Surface Methodology Behnken Box Design. The Box-Behnken design offers several advantages in Response Surface Methodology (RSM), mainly when using three independent and one response variable.

This efficient design requires fewer experimental runs than the central composite design (CCD), making it more cost-effective and less time-consuming. It strategically places experimental points to capture the interactions and quadratic effects of the variables without testing all possible combinations, thus avoiding extreme conditions. This means it does not include points at the corners of the experimental space, reducing the risk of impractical or unsafe conditions during experimentation [39].

Furthermore, the design is rotatable or nearly rotatable, ensuring that the prediction variance is relatively constant at equal distances from the center, leading to more reliable predictions for the degradation percentage. This characteristic allows for greater accuracy in exploring the response surface across different experimental conditions. Its suitability for fitting second-order (quadratic) models makes it effective for optimizing the degradation percentage of the photocatalyst weight, H_2O_2 concentration, and contact time, demonstrating the flexibility and efficiency of the Box-Behnken design in RSM studies. Additionally, the design reduces the number of required experimental runs compared to other designs, offering a more efficient approach to experimentation. By providing a comprehensive understanding of the interaction effects between the variables, the Box-Behnken design aids in identifying optimal operating conditions with fewer resources and time, making it ideal for process optimization in degradation studies [40]. Table 3 shows the design matrix in the form of independent variables (X_1, X_2, X_3), their ranges, and the resulting response variables (Y).

Table 3: Outline of experimental design with coded and un-coded values.

Design Point	Independent Variables in Coded Form			Independent Variables in their Natural Form			Response Variable
	X_1	X_2	X_3	X_1	X_2	X_3	Y
1	0	1	–1	1.0	0.3	90	86.25
2	1	0	–1	1.5	0.2	90	92.61
3	1	–1	0	1.5	0.1	120	91.25
4	–1	0	1	0.5	0.2	150	97.74
5	0	0	0	1.0	0.2	120	96.58
6	–1	–1	0	0.5	0.1	120	88.10
7	0	0	0	1.0	0.2	120	97.59
8	0	0	0	1.0	0.2	120	96.74
9	0	1	1	1.0	0.3	150	91.14
10	–1	1	0	0.5	0.3	120	90.68
11	0	–1	–1	1.0	0.1	90	69.86
12	1	1	0	1.5	0.3	120	94.98
13	0	–1	1	1.0	0.1	150	89.33
14	1	0	1	1.5	0.2	150	97.90
15	–1	0	–1	0.5	0.2	90	91.91

X_1 = Weight of photocatalyst (mg),
X_2 = Concentration of H_2O_2 (M)
X_3 = Time contact (minutes)
Y = Percentage of degradation (%)

The relationship between the response and independent variables is expressed in Equation (7). The positive sign of the coefficient in the equation above indicates a synergistic influence between the variables on the response, meaning that as these variables increase, the response improves. Conversely, the negative sign indicates an antagonistic influence, where an increase in the variables leads to a reduction in the response. This distinction between synergistic and antagonistic effects is critical for understanding how each variable contributes to the overall outcome and optimizing the conditions to achieve the desired response [41].

$$\%DE = -53.2 - 18.7X_1 + 502.9X_2 + 1.605X_3 + 10.36X_1{*}X_1 - 831X_2{*}X_2 - 0.00502X_3{*}X_3 + 5.7\,X_1{*}X_2 - 0.009\,X_1{*}X_3 - 1.215\,X_2{*}X_3 \quad (7)$$

Table 4 shows the analysis of variance (ANOVA) used to test the feasibility of the model used. If the *p*-value is less than 0.05, it indicates that the data is statistically significant [41]. In this study, the *p*-value for the independent variables of H_2O_2 concentration (X_2) and contact time (X_3) were 0.035 and 0.009, respectively. Both variables have *p*-values of less than 0.05, so it can be said that the concentration of H_2O_2 and contact time significantly affect the response, namely the % of dye degradation. The photocatalyst weight variable (X_1) has a *p*-value of 0.375, which is more than 0.05, so it can be said that the photocatalyst weight influences the degradation of tetramethylthionine chloride dye but is not significant. The same thing happens for the quadratic variable, while the interaction variable has an insignificant effect.

Table 4: Analysis of Variance (ANOVA).

Source	DF	F-Value	*p*-value
Model	9	7.93	0.017
X_1	1	0.95	0.375
X_2	1	8.23	0.035
X_3	1	17.25	0.009
$X_1{*}X_1$	1	2.71	0.160
$X_2{*}X_2$	1	27.93	0.003
$X_3{*}X_3$	1	8.27	0.035
$X_1{*}X_2$	1	0.04	0.856
$X_1{*}X_3$	1	0.01	0.932
$X_2{*}X_3$	1	5.83	0.061
Error	5		

The ANOVA test reveals that the concentration of H_2O_2 and contact time exert a considerable influence, both as independent variables and in their quadratic forms. These variables act as critical parameters that strongly affect the photodegradation of tetramethylthionine chloride dye. Their influence is crucial not only individually but also in terms of their non-linear effects, indicating that both the levels of these variables and their interactions contribute considerably to the efficiency of the degradation process. Understanding their influence allows for more precise optimization of the experimental conditions for maximum dye removal.

Figure 13 illustrates the 3D surface plots showing the influence of interactions between different variables on the degradation percentage. The white areas in the plots indicate the optimum conditions for each combination of variables.

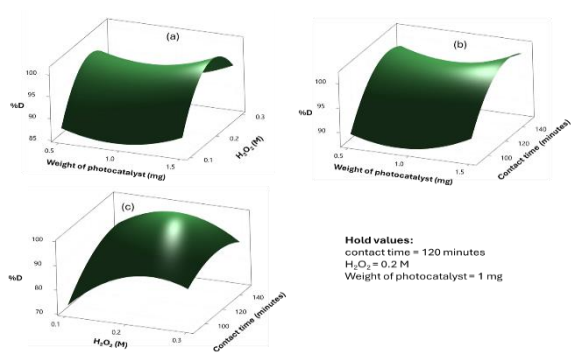

Figure 13: 3D surface plots showing the interaction effects of photocatalyst weight, H_2O_2 concentration, and contact time on degradation efficiency.

The first plot (Figure 13(a)), which shows the interaction between the photocatalyst weight and H_2O_2 concentration, reveals that as both variables increase, the degradation percentage also rises to an optimum point. The optimal region is observed at an H_2O_2 concentration ranging from 0.2 to 0.25 M and a photocatalyst weight between 1.35 to 1.50 mg.

The second plot (Figure 13(b)), showing the interaction between photocatalyst weight and contact time, indicates that higher degradation efficiency is achieved with a photocatalyst weight between 1.35 to 1.50 mg and a contact time ranging from 120 to 150 minutes. The plot suggests that increasing the photocatalyst weight and contact time contributes to a higher degradation percentage up to this optimal range.

The third plot (Figure 13(c)) displays the relationship between H_2O_2 concentration and contact time. The optimum degradation conditions are found at an H_2O_2 concentration of 0.20 to 0.26 M and a contact time between 110 and 150 min. These plots highlight that the highest degradation efficiency is achieved when the parameters are within these identified ranges, providing crucial guidance for optimizing experimental conditions.

Figure 14 shows the optimum conditions with the target response %D set to the maximum, which was then calculated statistically using the Response Optimizer feature in Minitab. The results indicate that the statistically optimal response can be achieved with the following conditions: A photocatalyst weight of Fe-PTC MOF at 1.5 mg, an H_2O_2 concentration of approximately 0.2 M, and a contact time of around 133 min.

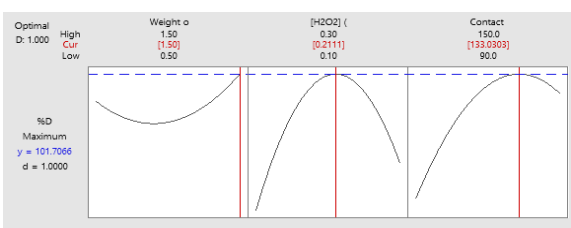

Figure 14: Response optimizer plot for optimal degradation conditions of tetramethylthionine chloride using Fe-PTC MOF as photocatalyst.

4 Conclusions

This study successfully synthesized and characterized Fe-PTC MOF as a highly efficient photocatalyst for the degradation of tetramethylthionine chloride (TMTC) in aqueous systems. With a degradation efficiency of 97% under visible light irradiation and the addition of H_2O_2, Fe-PTC MOF demonstrates strong potential to address the critical issue of dye contamination in textile wastewater. Its low bandgap energy (1.94 eV) enables effective utilization of visible light, providing a sustainable and cost-effective approach to photocatalytic wastewater treatment. Compared to conventional methods such as adsorption or coagulation, this approach offers the distinct advantage of breaking dyes into non-toxic compounds rather than transferring pollutants to another phase. However, this study is not without limitations. The photocatalytic performance was evaluated using a single dye model, and the material's long-term stability and reusability remain to be comprehensively investigated. Additionally, the scalability and efficiency of Fe-PTC MOF in treating natural wastewater systems have not been tested. Furthermore, the environmental impact of Fe-PTC MOF, including the potential leaching of iron or organic components into treated water, was not assessed. Future studies should focus on evaluating the stability of Fe-PTC MOF under operational conditions, monitoring potential leaching, and ensuring compliance with water quality standards.

Acknowledgments

This study was supported by The Indonesia Endowment Funds for Education (LPDP) for granting doctoral scholarship to the first author.

Author Contributions

M.F.: conceptualization, investigation, methodology, data analysis, writing an original draft; A.Z.: research design, conceptualization, data curation, reviewing, and editing; J.G.: conceptualization, data curation, reviewing, and editing. All authors have read and agreed to the published version of the manuscript.

Conflicts of Interest

The authors declare no conflict of interest.

References

[1] T. Xia, Y. Lin, W. Li, and M. Ju, "Photocatalytic degradation of organic pollutants by MOFs based materials: A review," *Chinese Chemical Letters*, vol. 32, no. 10, pp. 2975–2984, Oct. 2021, doi: 10.1016/j.cclet.2021.02.058.

[2] K. Siddique, M. Rizwan, M. J. Shahid, S. Ali, R. Ahmad, and H. Rizvi, "Textile wastewater treatment options: A critical review," *Enhancing Cleanup of Environmental Pollutants*, vol. 2, pp. 183–207, 2017, doi: 10.1007/978-3-319-55423-5_6.

[3] M. R. Al-Mamun, S. Kader, M. S. Islam, and M. Z. H. Khan, "Photocatalytic activity improvement and application of UV-TiO_2 photocatalysis in textile wastewater treatment: A review," *Journal of Environmental Chemical Engineering*, vol. 7, no. 5, Oct. 2019, Art. no. 103248, doi: 10.1016/J.JECE.2019.103248.

[4] M. Saeed, M. Usman, and A. ul Haq, "Catalytic Degradation of Organic Dyes in Aqueous Medium," in *Photochemistry and Photophysics - Fundamentals to Applications*. London, UK: InTech, 2018. doi: 10.5772/intechopen.75008.

[5] A. Hardian, R. H. Putri, S. Budiman, and D. G. Syarif, "Sintesis keramik komposit ZrO_2-$ZnFe_2O_4$ sebagai fotokatalis magnetik untuk degradasi metilen biru," *ALCHEMY Jurnal Penelitian Kimia*, vol. 17, no. 1, pp. 43–53, 2021, doi: 10.20961/alchemy.17.1.39240.43-53.

[6] D. Mukherjee, B. Van der Bruggen, and B. Mandal, "Advancements in visible light responsive MOF composites for photocatalytic decontamination of textile wastewater: A review," *Chemosphere*, vol. 295, May 2022, Art. no. 133835, doi 10.1016/j.chemosphere.2022.133835.

[7] J. Bedia, V. Muelas-Ramos, M. Peñas-Garzón, A. Gómez-Avilés, J. J. Rodríguez, and C. Belver, "A review on the synthesis and characterization of metal-organic frameworks for photocatalytic water purification," *Catalysts*, vol. 9, no. 1, p. 52, 2019, doi: 10.3390/catal9010052.

[8] S. A. Younis, E. E. Kwon, M. Qasim, K.-H. Kim, T. Kim, D. Kukkar, X. Dou, and I. Ali, "Metal-organic framework as a photocatalyst: Progress in modulation strategies and environmental/energy applications," *Progress in Energy and Combustion Science*, vol. 81, Nov. 2020, Art. no. 100870, doi: 10.1016/j.pecs.2020.100870.

[9] A. Zulys, A. Adawiah, J. Gunlazuardi, and M. D. L. Yudhi, "Light-harvesting metal-organic frameworks (MOFs) La-PTC for photocatalytic dyes degradation," *Bulletin of Chemical Reaction Engineering & Catalysis*, vol. 16, no. 1, pp. 170–178, 2021, doi: 10.9767/bcrec.16.1.10309.170-178.

[10] A. Adawiah, R. N. Fitria, N. Saridewi, F. M. Azhar, M. S. Gunawan, and S. Komala, "Synthesis glycine-modulated metal-organic framework Cr-PTC-Gly for synergetic methylene blue adsorption and photodegradation under visible light irradiation," *Molekul*, vol. 17, no. 3, pp. 374–382, 2022, doi: 10.20884/1.jm.2022.17.3.6126.

[11] N. Saridewi, F. M. Azhar, P. A. Abdillah, A. Zulys, S. Nurbayti, L. Tulhusna, and A. Adawiah, "Synthesize metal-organic frameworks from chromium metal ions and ptcda ligands for methylene blue photodegradation," *Rasayan Journal of Chemistry*, vol. 15, no. 4, pp. 2544–2550, 2022, doi: 10.31788/RJC.2022.1547046.

[12] A. Adawiah, W. Oktavia, N. Saridewi, F. M. Azhar, R. N. Fitria, M. S. Gunawan, S. Komala, and A. Zulys, "Synthesis metal-organic framework (MOFs) Cr-PTC-HIna modulated isonicotinic acid for methylene blue photocatalytic degradation," *Bulletin of Chemical Reaction Engineering & Catalysis*, vol. 17, no. 2, pp. 383–393, 2022, doi: 10.9767/bcrec.17.2.13930.383-393.

[13] A. Adawiah, M. D. L. Yudhi, and A. Zulys, "Photocatalytic degradation of methylene blue and methyl orange by Y-PTC metal-organic framework," *Jurnal Kimia Valensi*, vol. 7, no. 2, pp. 129–141, 2021, doi: 10.15408/jkv.v7i2.22267.

[14] M. Fathurrahman, A. Zulys, and J. Gunlazuardi, "Fotodegradasi metilen biru oleh metal organic framework (MOF) Fe-PTC dengan penambahan H_2O_2 dan dioptimasi menggunakan desain box behnken," *Jurnal Kartika Kimia*, vol. 6, no. 2, pp. 131–144, 2024, doi: 10.26874/jkk.v6i2.228.

[15] A. Zulys, M. Defania, J. Gunlazuardi, and Adawiah, "Glycine-modulated zirconium perylene-based metal-organic framework for rhodamin B photocatalytic degradation," *Molekul*, vol. 18, no. 3, pp. 497–507, 2023, doi: 10.20884/1.jm.2023.18.3.9126.

[16] M. T. D. C. Español, E. R. J. G. Garcia, L. A. V. Maligaya, C. M. S. Santos, J. A. H. Santos, N. G. Suarnaba, R. V. C. Rubi, and R. Raguindin, "Ultrasound-assisted biomimetic synthesis of

MOF-Hap nanocomposite via 10xSBF-like for the photocatalytic degradation of metformin," *Applied Science and Engineering Progress*, vol. 17, no. 2, 2024, Art. no. 7251, doi: 10.14416/j.asep.2023.11.002.

[17] J. M. Seco, E. S. Sebastián, J. Cepeda, B. Biel, A. S. Castillo, B. Fernández, D. P. Morales, M. Bobinger, S. G. Ruiz, F. C. Loghin, A. Rivadeneyra, and A. R. Diéguez, "A potassium metal-organic framework based on perylene-3,4,9,10-tetracarboxylate as sensing layer for humidity actuators," *Scientific Reports*, vol. 8, no. 1, 2018, Art. no. 14414, doi: 10.1038/s41598-018-32810-7.

[18] L. C. Christina, J. Gunlazuardi, and A. Zulys, "Synthesis and characterization of lanthanide metal-organic framework with perylene 3,4,9,10-tetracarboxylate ligand," in *IOP Conference Series: Materials Science and Engineering*, 2020, doi: 10.1088/1757-899X/902/1/012046.

[19] A. Zulys, A. Adawiah, and N. Nasruddin, "Efficient degradation of methylene blue using La-PTC-HIna/$Ti_3C_2T_x$ MXene: Adsorption and photocatalytic degradation," *Indonesian Journal of Chemistry*, vol. 22, no. 5, pp. 1195–1204, 2022, doi: 10.22146/ijc.71692.

[20] S. Demirci, G. Gizer, O. Polat, M. K. Ram, and N. Sahiner, "The synthesis and characterization of PTCDA-Co(II), and PTCDA-La(III) fluorescent MOFs," *Inorganica Chimica Acta*, vol. 542, Nov. 2022, Art. no. 121102, doi: 10.1016/j.ica.2022.121102.

[21] A. Zulys, D. Asrianti, and J. Gunlazuardi, "Synthesis and characterization of metal-organic frameworks based on nickel and perylene dyes as water splitting photocatalyst," *AIP Conference Proceedings*, vol. 2243, pp. 5–9, 2020, doi: 10.1063/5.0005001.

[22] S. Sowmiyha, V. V. Kumar, J. Pitchaimani, V. Madhu, R. Thiagarajan, N. S. Subramanian, and S. P. Anthony, "Self-assembly of water-soluble perylene tetracarboxylic acid with metal cations: Selective fluorescence sensing of Cu^{2+} and Pb^{2+} ions in paper strips, zebrafish, and yeast," *Journal of Luminescence*, vol. 203, pp. 42–49, 2018, doi: 10.1016/j.jlumin.2018.06.026.

[23] I. Susanti, R. M. Iqbal, R. A. Rachman, and T. A. Pradana, "Photocatalytic activity and kinetic study of methylene blue degradation using N-doped TiO_2 with zeolite-NaY," *CHEESA: Chemical Engineering Research Articles*, vol. 4, no. 2, p. 75, Aug. 2021, doi: 10.25273/cheesa.v4i2.7646.75-81.

[24] N. N. Bahrudin, "Evaluation of degradation kinetic and photostability of immobilized TiO_2/activated carbon bilayer photocatalyst for phenol removal," *Applied Surface Science Advances*, vol. 7, Feb. 2022, Art. no. 100208, doi: 10.1016/j.apsadv.2021.100208.

[25] D. L. Pavia, G. M. Lampman, and G. S. Kriz, *Introduction to Spectroscopy: A Guide for Students of Organic Chemistry*, 5th ed. USA: Cengage Learning, pp. 14–87, 2009.

[26] O. S. Bull, I. Bull, G. K. Amadi, C. Obaalologhi Odu, and E. O. Okpa, "A review on metal-organic frameworks (MOFS), synthesis, activation, characterization, and application," *Oriental Journal of Chemistry*, vol. 38, no. 3, pp. 490–516, Jun. 2022, doi: 10.13005/ojc/380301.

[27] R. Ediati, M. Kahardian, and D. Hartanto, "Pengaruh perbandingan pelarut etanol dan dimetilformamida pada sintesis *Metal Organik Framework* HKUST-1," *Akta Kimia Indonesia*, vol. 1, no. 1, p. 25, Nov. 2016, doi: 10.12962/j25493736.v1i1.1425.

[28] N. Riezzati, Y. K. Krisnandi, and A. Zulys, "Metal-organic frameworks of lanthanum and iron using BDC linker as catalysts for glucose conversion into 5-hydroxymethylfurfural (5-HMF)," in *IOP Conference Series: Materials Science and Engineering*, vol. 902, 2020, doi: 10.1088/1757-899X/902/1/012044.

[29] A. Kudo and Y. Miseki, "Heterogeneous photocatalyst materials for water splitting," *Chemical Society Reviews*, vol. 38, no. 1, pp. 253–278, 2009, doi: 10.1039/b800489g.

[30] R. Seetharaj, P. V. Vandana, P. Arya, and S. Mathew, "Dependence of solvents, pH, molar ratio and temperature in tuning metal-organic framework architecture," *Arabian Journal of Chemistry*, vol. 12, no. 3, pp. 295–315, 2019, doi: 10.1016/j.arabjc.2016.01.003.

[31] L. L. Zulfa, R. Ediati, A. R. P. Hidayat, R. Subagyo, N. Faaizatunnisa, Y. Kusumawati, D. Hartanto, N. Widiastuti, W. P. Utomo, and M. Santoso "Synergistic effect of modified pore and heterojunction of MOF-derived α-Fe_2O_3/ZnO for superior photocatalytic degradation of methylene blue," *RSC Advances*, vol. 13, no. 6, pp. 3818–3834, Jan. 2023, doi: 10.1039/d2ra07946a.

[32] Y. Chen, B. Zeng, L. Lai, L. Luo, P. Xie, Q. Shao, Z. Liu, and J. Ma, "Sulfite activation using FeO as a source of ferrous ions for fluoxetine

degradation: A collaborated experimental and DFT study," *Chemical Engineering Journal*, vol. 441, Aug. 2022, Art. no. 135960, doi: 10.1016/j.cej.2022.135960.

[33] F. Ambroz, T. J. Macdonald, V. Martis, and I. P. Parkin, "Evaluation of the BET theory for the characterization of meso and microporous MOFs," *Small Methods*, vol. 2, no. 11, 2018, Art. no. 1800173, doi: 10.1002/smtd.201800173.

[34] M. M. Karkare, "The Direct transition and not Indirect transition, is more favorable for Band Gap calculation of Anatase TiO_2 nanoparticles," *International Journal of Scientific & Engineering Research*, vol. 6, no. 12, pp. 48–53, 2015.

[35] Q. He, Y. Fu, X. Ge, A. M. Al-Enizi, A. Nafady, Q. Wang, and S. Ma "Facile fabrication of Fe-BDC/Fe-2MI heterojunction with boosted photocatalytic activity for Cr(VI) reduction," *Journal of Environmental Chemical Engineering*, vol. 9, no. 5, Oct. 2021, Art. no. 105961, doi: 10.1016/j.jece.2021.105961.

[36] C. K. Lin, D. Zhao, W. Y. Gao, Z. Yang, J. Ye, T. Xu, Q. Ge, S. Ma, and D. J. Liu, "Tunability of band gaps in metal-organic frameworks," *Inorg Chem*, vol. 51, no. 16, pp. 9039–9044, Aug. 2012, doi: 10.1021/ic301189m.

[37] A. Zulys, Q. A'Yun, and J. Gunlazuardi, "Synthesis of metal-organic frameworks based on lanthanum metal and perylene ligand as photocatalyst for hydrogen gas production," in *AIP Conference Proceedings*, American Institute of Physics Inc., 2020, Art. no. 020034, doi: 10.1063/5.0005000.

[38] L. J. Kusumawardani, T. Widyyanti, A. Iryani, U. Hasanah, and N. Nurlela, "Optimization and mechanism elucidation of catalytic photodegradation methylene blue by TiO_2/zeolite coal fly ash nanocomposite under H_2O_2 presence," *Jurnal Sains Natural*, vol. 14, no. 2, pp. 98–108, 2024, doi: 10.31938/jsn.v14i2.722

[39] R. H. Myers, D. C. Montogomery, and C. M. A. Cook, *Response Surface Methodology: Process and Product Optimization Using Designed Experiments*, 3rd ed. USA: John Wiley & Sons, Inc.,2009, pp. 281–336.

[40] M. A. Bezerra, R. E. Santelli, E. P. Oliveira, L. S. Villar, and L. A. Escaleira, "Response surface methodology (RSM) as a tool for optimization in analytical chemistry," *Talanta*, vol. 76, no. 5, pp. 965–977, Sep. 2008, doi: 10.1016/j.talanta.2008.05.019.

[41] L. A. Indriyani, Z. Arif, R. Linda, H. Purwaningsih, and M. Rafi, "Pengoptimuman Kondisi Adsorpsi Cd(II) oleh Adsorben Berbasis Silika Termodifikasi Glisina Menggunakan *Central Composite Design*," *Jurnal Kimia Sains dan Aplikasi*, vol. 22, no. 5, pp. 184–191, Sep. 2019, doi: 10.14710/jksa.22.5.184-191.